

Maximum *a posteriori* blind image deconvolution with Huber–Markov random-field regularization

Zhimin Xu and Edmund Y. Lam*

Imaging Systems Laboratory, Department of Electrical and Electronic Engineering, The University of Hong Kong, Pokfulam Road, Hong Kong

*Corresponding author: elam@eee.hku.hk

Received January 9, 2009; revised April 7, 2009; accepted April 7, 2009;
posted April 9, 2009 (Doc. ID 106175); published April 30, 2009

We propose a maximum *a posteriori* blind deconvolution approach using a Huber–Markov random-field model. Compared with the conventional maximum-likelihood method, our algorithm not only suppresses noise effectively but also significantly alleviates the artifacts produced by the deconvolution process. The performance of this method is demonstrated by computer simulations. © 2009 Optical Society of America
OCIS codes: 100.1455, 100.1830, 100.2000, 100.3020, 100.3190.

Digital images are obtained in areas ranging from everyday photography to astronomy, remote sensing, medical imaging, and microscopy. In each case, there is an underlying object or scene we wish to observe. However, the observation process is seldom perfect; there is always uncertainty in the measurements, manifested as blur, noise, and other degradations in the recorded images. In the case of a linear shift-invariant imaging system, the relation between the observed image i and the true image o in the same coordinate frame is a convolution. That is,

$$i(\mathbf{x}) = h(\mathbf{x}) * o(\mathbf{x}), \quad (1)$$

where h represents the point-spread function (PSF), \mathbf{x} refers to a lexicographically ordered vector of the pixel coordinates in a 2D image, and the operator $*$ denotes 2D convolution. In realistic scenarios, we must also consider noise, which is often modeled by a specific statistical distribution.

Our objective is to estimate $o(\mathbf{x})$ and $h(\mathbf{x})$ based on degraded image $i(\mathbf{x})$ and prior information about the true imaged scene. This estimate process is also known as blind image deconvolution. Over the years, many blind deconvolution algorithms have been developed, such as iterative [1–3] and noniterative methods [4,5] (for a review see [6]). In this Letter, the Bayesian image deconvolution model is used. Based on Bayes’s rule, there are two possible estimates: the maximum likelihood (ML) estimate and the maximum *a posteriori* (MAP) estimate. The ML method initially proposed by Richardson [7] and Lucy [8] is the most well known for image deblurring. In [9], Fish *et al.* extended their idea to image reconstruction in the “blind” situation. Nevertheless, owing to the ill-posed nature of inverse problems, these algorithms often lack stability and uniqueness. The MAP method is closely related to the method of the ML estimate, but the incorporation of a prior distribution over the original scene can be seen as a regularization of ML estimate, i.e.,

$$\hat{\theta} = \arg \max_{\theta} [p(i|\theta)p(\theta)] \quad (2)$$

$$= \arg \max_{\theta} [\log p(i|\theta) + \log p(\theta)], \quad \theta = \{o, h\}, \quad (3)$$

where the set θ contains the unknown parameters for the blind deconvolution problem and p denotes probability.

Considering the cases where the data is contaminated by Poisson noise, such as in astronomy and microscopy, the intensity of each pixel \mathbf{x} in the observed image is a random variable that follows an independent Poisson distribution of a mean $[h(\mathbf{x}) * o(\mathbf{x})]$. The likelihood can then be written as

$$p(i|o, h) = \prod_{\mathbf{x}} \frac{[h(\mathbf{x}) * o(\mathbf{x})]^{i(\mathbf{x})}}{i(\mathbf{x})!} \exp\{-[h(\mathbf{x}) * o(\mathbf{x})]\}. \quad (4)$$

Unpleasant artifacts (e.g., ringing) from the deconvolution process are often inevitable because of the loss of the high-frequency component in the reconstructed image. Besides, noise and discretization of the image and the PSF amplify errors in the deconvolution process. For instance, from the simulation, it can be found that too many iterations in the Richardson–Lucy algorithm (RLA) will result in more “ringing” artifacts, especially on the location of intensity discontinuities. In this Letter, we use a non-Gaussian Markov random-field (MRF) model to suppress the artifacts. MRF models are used in image processing to define a distribution over neighborhoods for describing the local structure of an image, and that distribution is used to solve the image reconstruction problem. Here we use a special form of Gibbs distribution to characterize the distribution of the MRF. This has been shown to successfully model both the smooth regions and discontinuities of images in image decompression [10] and superresolution image reconstruction from multiple low-resolution images [11]. In [12], a similar distribution is used for preserving edges in image restoration, but the context is different from ours as we deal with Poisson noise in a “blind” situation. The form of the distribution is explicitly given by

$$p(o) = \frac{1}{Z} \exp \left[-\lambda \sum_{c \in C} \rho(a_c^T o) \right], \quad (5)$$

where $\lambda > 0$, Z is a normalizing constant, a_c is a linear operator defined on a local group of points c called a clique, and the function $\rho(u)$, which is also called the Huber function, is defined as

$$\rho(u) = \begin{cases} u^2, & |u| \leq \xi \\ \xi^2 + 2\xi(|u| - \xi), & |u| > \xi \end{cases} \quad (6)$$

The Huber function is a good compromise between L_1 and L_2 norms. The Huber threshold ξ controls the transition between these two norms. For small u , the Huber function becomes the usual L_2 least-squares penalty function, which exhibits the stability and rapid convergence characteristics; for large u , it reduces to the noise insensitive L_1 penalty function. To include the measurement of discontinuities into the statistical model, we use the linear operator a_c to measure inconsistency of a local area.

Combining with the prior distribution presented above, from Eq. (3), we can get the negative log-likelihood

$$\mathcal{J}(\theta) = \sum_{\mathbf{x}} \left\{ [h(\mathbf{x}) * o(\mathbf{x})] - i(\mathbf{x}) + i(\mathbf{x}) \log \frac{i(\mathbf{x})}{h(\mathbf{x}) * o(\mathbf{x})} + \lambda \sum_{c \in C} \rho[a_c^T o(\mathbf{x})] \right\}. \quad (7)$$

Maximizing $[\log p(i|\theta) + \log p(\theta)]$ is equivalent to minimizing $\mathcal{J}(\theta)$. According to the expectation-maximization (EM) algorithm, the numerical iterative algorithm is then obtained,

$$\begin{aligned} h_t^{(k+1)}(\mathbf{x}) &= \hat{h}^{(k)}(\mathbf{x}) \left\{ \hat{o}^{(k)}(-\mathbf{x}) * \left[\frac{i(\mathbf{x})}{\hat{h}^{(k)}(\mathbf{x}) * \hat{o}^{(k)}(\mathbf{x})} \right] \right\}, \\ \hat{h}^{(k+1)}(\mathbf{x}) &= \frac{h_t^{(k+1)}(\mathbf{x})}{\left[\sum_{\mathbf{x}} h_t^{(k+1)}(\mathbf{x}) \right]}, \end{aligned} \quad (8)$$

$$\begin{aligned} \hat{o}^{(k+1)}(\mathbf{x}) &= \hat{o}^{(k)}(\mathbf{x}) \left\{ \hat{h}^{(k+1)}(-\mathbf{x}) * \left[\frac{i(\mathbf{x})}{\hat{h}^{(k+1)}(\mathbf{x}) * \hat{o}^{(k)}(\mathbf{x})} \right] \right\} \\ &\times \frac{1}{\left\{ 1 + \lambda \sum_{c \in C} a_c \rho'[a_c^T \hat{o}^{(k)}(\mathbf{x})] \right\}}, \end{aligned} \quad (9)$$

where the superscript indexes the number of the iteration and $\rho'(u)$ refers to the first derivative of the function $\rho(u)$,

$$\rho'(u) = \begin{cases} 2u, & |u| \leq \xi \\ 2\xi \frac{u}{|u|}, & |u| > \xi \end{cases}. \quad (10)$$

For the selection of the relaxation factor λ and the Huber threshold ξ , we use the method proposed in [13] as a reference.

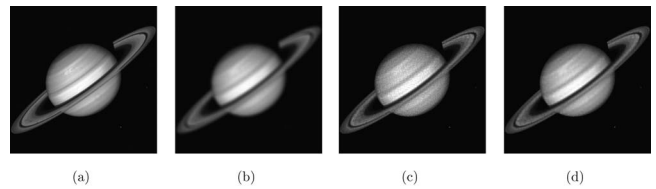


Fig. 1. Restorations of a simulated astronomy image: (a) original image, (b) blurred and noisy image, (c) image restored with RLA, and (d) image restored with our approach.

To demonstrate the effectiveness of our method, we execute simulations with two kinds of images under the Poisson noise process. First, we take the situation in astronomical image processing into account. It is well known that the noise associated with the collection of an astronomical image by a CCD camera is mostly Poissonian. A gray level image “Saturn” of size 256×256 is used. This image is degraded by an 8×8 Gaussian blur kernel. Then simulated photon noise is added to the degraded image by generating a random number obeying a Poisson distribution with the mean of the pixel value of this noiseless degraded image. The numbers generated for all the pixels then form the observed image. We compare our approach with the conventional RLA. Figures 1(a)–1(d) show the original image, the blurred and noisy image, the restored image with standard RLA, and the result with our algorithm, respectively. In the simulation we choose $\lambda = 0.06$, $\xi = 0.008$, and 200 iterations. As for the linear operator a_c , a 3×3 window is used for consistency measure,

$$a_c = \begin{bmatrix} 1 & & \\ -\frac{1}{2} & -1 & -\frac{1}{2} \\ -1 & 6 & -1 \\ -\frac{1}{2} & -1 & -\frac{1}{2} \end{bmatrix}. \quad (11)$$

Comparing Fig. 1(c) with Fig. 1(d), it can be found that the artifacts on the surface of the planet, which are caused by the noise, are apparently reduced. To measure the improvement in the restored image quality, the normalized mean-square error (NMSE) can be used and is defined as

$$\text{NMSE} = \frac{\sum_{\mathbf{x}} [\hat{o}(\mathbf{x}) - o(\mathbf{x})]^2}{\sum_{\mathbf{x}} [o(\mathbf{x})]^2}. \quad (12)$$

Here, $\hat{o}(\mathbf{x})$ stands for the restored image. The NMSE of two different estimates versus the iteration number are shown in Fig. 2, where the convergence is also highlighted.

We further illustrate the capabilities of our approach for a scenario in microscopy. Owing to photon-limited detection, microscopical images (e.g., confocal microscopical images) are always corrupted by Poisson noise. We use a synthetic phantom image composed of five geometrical patterns for simulation.

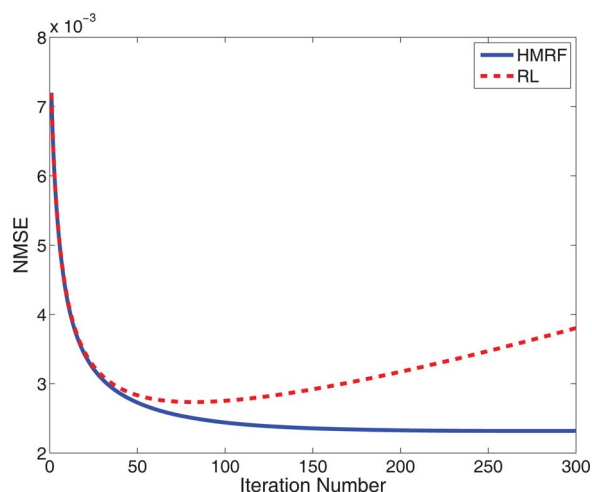


Fig. 2. (Color online) NMSE of RLA and our approach.

This kind of image has been adopted to evaluate the performances of image-restoration algorithms in terms of qualitative and also quantitative measures [14]. The experimental settings are the same as for “Saturn.” As for the parameter, we use $\lambda=0.8$ and $\xi=0.006$. The deconvolution results of standard RLA and our approach are shown in Figs. 3(c) and 3(d). In the RLA deconvolution, many artifacts, such as speckles and ringings, appear inside the shapes and near their edges. However, these are remarkably attenuated in the result with our method.

In conclusion, a MAP-based methodology for blind deconvolution is proposed. It uses a non-Gaussian MRF model based on the Huber function for stable image reconstruction. For the sake of stability and uniqueness, many algorithms have been proposed to regularize RLA, such as L_2 norm and L_1 norm. Yet

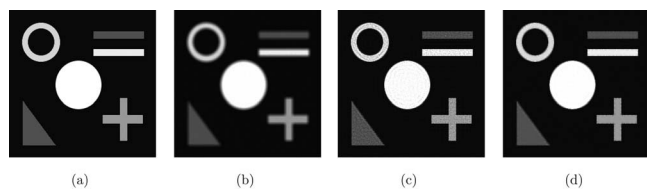


Fig. 3. Restorations of a synthetic phantom image: (a) original image, (b) blurred and noisy image, (c) image restored with RLA, and (d) image restored with our approach.

these often oversmooth the edges in an image or are not readily computed. Because of the Huber function’s good combination of L_1 and L_2 norms, this property helps to maintain robustness in the presence of noise and discontinuities of an image like an L_1 measure, and also stability and rapid convergence characteristic of an L_2 measure. Meanwhile, the incorporation of the interaction between pixels adaptively adjusts the regularization during the deconvolution process. We have presented results on two different kinds of data. Comparing the results with traditional deconvolution techniques (e.g., RLA), our algorithm remarkably alleviates the noticeable artifacts in the reconstructed images.

This work was supported in part by the Research Grants Council of the Hong Kong Special Administrative Region, China under projects HKU 713906 and 713408.

References

1. J. H. Seldin and J. R. Fienup, *J. Opt. Soc. Am. A* **7**, 428 (1990).
2. E. Y. Lam and J. W. Goodman, *J. Opt. Soc. Am. A* **17**, 1177 (2000).
3. E. Y. Lam, *IEEE Trans. Circuits Syst. II* **54**, 52 (2007).
4. A. S. Carasso, *SIAM J. Appl. Math.* **61**, 1980 (2001).
5. J. N. Caron, N. M. Namazi, and C. J. Rollins, *Appl. Opt.* **41**, 6884 (2002).
6. D. Kundur and D. Hatzinakos, *IEEE Signal Process. Mag.* **13**, 43 (1996).
7. W. H. Richardson, *J. Opt. Soc. Am.* **62**, 55 (1972).
8. L. B. Lucy, *Astron. J.* **79**, 745 (1974).
9. D. A. Fish, A. M. Brinicombe, E. R. Pike, and J. G. Walker, *J. Opt. Soc. Am. A* **12**, 58 (1995).
10. T. P. O’Rourke and R. L. Stevenson, *IEEE Trans. Circuits Syst. Video Technol.* **5**, 490 (1995).
11. F. Šroubek, J. Flusser, and G. Cristóbal, in *Blind Image Deconvolution: Theory and Application*, P. Campisi and K. Egiazarian, eds. (CRC Press, 2007), pp. 317–348.
12. R. Pan and S. J. Reeves, *IEEE Trans. Image Process.* **15**, 3728 (2006).
13. H. He and L. P. Kondi, in *Proceedings of 2003 International Conference on Image Processing* (2003), Vol. 2, p. 933.
14. N. Dey, L. Blanc-Feraud, C. Zimmer, P. Roux, Z. Kam, J.-C. Olivo-Marin, and J. Zerubia, *Microsc. Res. Tech.* **69**, 260 (2006).